Fast Wave Power Flow Along SOL Field Lines in NSTX*

R. J. Perkins[1], J-W. Ahn[2], R. E. Bell[1], A. Diallo[1], S. Gerhardt[1], T. K. Gray[2], D. L. Green[2], E. F. Jaeger[3], J. C. Hosea[1], M. A. Jaworski[1], B. P. LeBlanc[1], G. J. Kramer[1], A. McLean[2], R. Maingi[2], C. K. Phillips[1], L. Roquemore[1], P.M. Ryan[2], S. Sabbagh[4], F. Scotti[1], G. Taylor[1], J. R. Wilson[1]

[1]Princeton Plasma Physics Laboratory, Princeton, NJ

[2]Oak Ridge National Laboratory, Oak Ridge, TN

[3]XCEL Engineering Inc., Oak Ridge, TN

[4]Columbia University, New York, NY

E-mail contact of main author: rperkins@pppl.gov

Abstract. The efficiency of fast wave (FW) heating and current drive can be reduced by a number of edge RF power loss processes in the vicinity of the antenna and in the scrape off layer (SOL), prior to the RF power reaching the core plasma inside the last closed flux surface (LCFS). These processes include sheath dissipation by near fields on and in the vicinity of the antenna, propagation of power on open field lines to the divertor regions, and possibly others. These edge losses subtract directly from the RF power deposited inside the LCFS and must be studied and then minimized in order to optimize fast wave heating and current drive performance generally. On NSTX up to 60% of the HHFW power coupled from the antenna has been observed to be lost to the SOL regions. A large part of this edge power loss is deposited in bright spirals on the divertor floor and ceiling, reaching up to ~ 2 MW/m^2 of localized heat deposition for ~ 2 MW of coupled antenna power. Magnetic field line mapping using the SPIRAL code shows that the spirals are caused by HHFW power flowing along open field lines that pass in front of the antenna at radii between the antenna and the LCFS. The spiraled geometry occurs because the field lines strike the divertor regions further around toroidally and further inward in major radius as the radii of the lines in the SOL at the antenna midplane approach the LCFS. Magnetic pitch scans show that the spirals move inward in major radius in the divertor regions at a given toroidal location with increasing pitch, as observed with cameras, tile currents, and Langmuir probes. The magnetic mappings track this behavior quite well. This one-to-one mapping of edge power flow from the SOL in front of the antenna to the divertor region should serve to verify advanced RF codes for the SOL against power flow along the field lines. Such codes then can be used to understand this edge power loss process and to assure minimization of RF heat deposition and erosion in the divertor region on ITER.

1. Introduction

Plasma heating using waves in the ion-cyclotron range of frequencies (ICRF) will be a primary heating scheme on ITER, where up to 20 MW of ICRF power is planned [1]. Effectively coupling the ICRF power from the sources to the core plasma is a major goal, and traditional issues include maintaining high antenna loading by keeping the plasma separatrix to antenna gap as small as possible and/or the edge density as large as permitted, losses near the antenna structures such as RF-sheath enhanced bombardment [2,3] and parametric decay instability (PDI) [4,5], and multi-pass dampening where waves that penetrate the core damp out at the plasma edge rather than in the core plasma [6]. However, significant losses can also occur directly in the SOL as the waves propagate away from the antenna; such losses can create situations of poor core heating even with high antenna loading and must be subtracted out before multi-pass dampening is considered.

On the National Spherical Torus Experiment (NSTX), the heating and current-drive efficiencies of the high-harmonic fast-wave (HHFW) system are significantly lowered due to

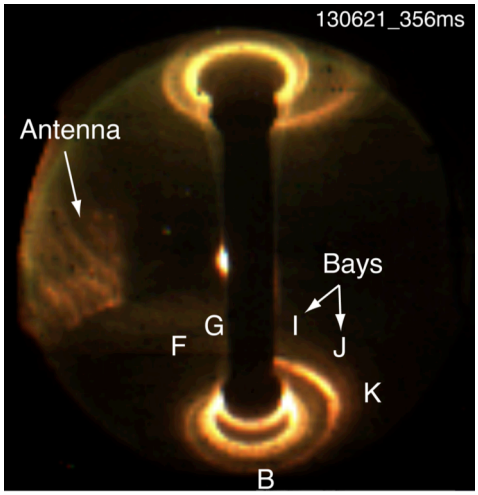

Figure 1. Strong interactions of the HHFW power and the edge plasma are clearly seen in this midplane visible-light image of the RF-induced streak and resulting spirals on the upper and lower divertor for an ELM-free H-mode plasma with P_{RF} = 1.8 MW. The conditions for shot 130621 are those detailed in Fig. 4 of Ref. 4: ϕ_{ANT} = -90°, P_{NB} = 2 MW, I_P = 1 MA, B_ϕ = 0.55 T.

interactions of the waves with the scrape-off layer (SOL) plasma [7,8]. These reductions in heating efficiencies are accompanied by bright streaks emanating from the antenna region and terminating on the upper and lower divertor in bright and hot spirals [9,10] (Fig. 1 and comparable in-vessel view of Fig. 2). Infrared (IR) camera measurements of these spirals show a significant RF-induced heat flux to the divertor, up to 2 MW/m^2 [10]. This indicates that a significant part of the HHFW power missing from the core is coupling directly to the SOL and is being deposited on the divertor. The heating efficiency is a strong function of the toroidal wavenumber, k_ϕ, selectively launched at the antenna, and edge density [7-10]. Figure 1 shows the spirals for the k_ϕ = -8 m^{-1} (-90° phasing between antenna straps) case of shot 130621 in Fig. 4 of Ref. 7 for which ~ 40% of the RF power coupled from the antenna reached the core plasma while ~ 60% was lost to the SOL. The background is relatively dark outside the spiral zones and antenna face for this ELM-free H-mode case. Importantly, the flow of the HHFW power from the midplane to the divertor in the SOL is largely along field lines [12], as has been determined by field-line mapping using the SPIRAL code [13], and occurs along all SOL field lines passing in front of the antenna, not just those connected to antenna components.

This paper uses the field-line mapping to map the IR divertor measurements of RF-induced heat flux back to the midplane, giving the radial profile of HHFW power coupled to SOL field lines in front of the antenna. For the case of Fig. 1, this procedure yields a power profile with relatively strong coupling ~ 1 cm inboard of the antenna and again a few millimeters outboard of the LCFS and relatively weak coupling in between. This suggests that the underlying mechanism behind this loss cannot be localized to the antenna components. It would appear that the underlying cause is fast-wave propagation in the SOL, with the low-density plasma between the antenna and LCFS acting in effect as a waveguide. Evidence for this behavior is found in the relationship between heating efficiency, edge density, and the onset density for perpendicular fast-wave propagation [7,8]. The results for power flow in the SOL resulting in localized heat deposition in the divertor region presented here suggest a radial standing wave pattern in the SOL channel between the very steep density gradient at the LCFS and the perpendicular fast wave cutoff/vessel wall. These results are important for verifying advanced RF codes, as these edge losses are readily apparent under NSTX conditions. Once these codes can predict the amount of fast wave power coupled to the SOL [14], they can be used for determining the underlying cause and for understanding how to minimize this direct SOL power loss for fast-wave heating, generally.

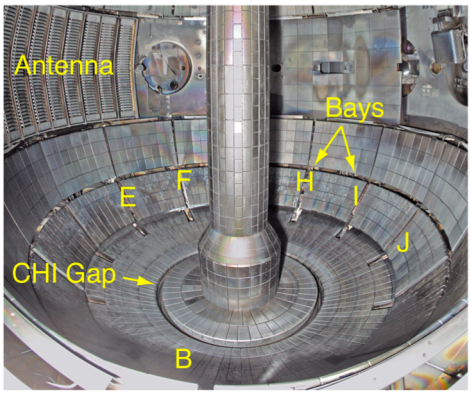

Figure 2. Vessel image showing position of the antenna, tiles, CHI gap [11], and toroidal bay locations. View rotated 30° toroidally relative to that of Fig. 1.

2. Field-line mapping and HHFW power flow in the SOL

HHFW power flows in the SOL mainly along the magnetic field, as is evidenced by comparing SOL field-line mapping to experimental measurements of RF-induced effects in the divertor regions. The following sections describe the field-line mapping procedure and the comparisons with data.

2.1. Field-line mapping using the SPIRAL code

Field-line mapping is done using the SPIRAL code, a full-orbit particle code [13]. The particle orbits produced with SPIRAL can be taken as proxies for the field lines because the particles are launched with velocities parallel to the magnetic field, which minimizes grad-B drifts, and with low speeds (1 eV deuterons), which minimizes curvature drifts. In this paper, field lines are tracked from the midplane in front of the antenna (which has a 90° toroidal span) to the point at which they strike the divertor region. Let R_{SOL} denote the major radius of a field line at the midplane. Figure 3 provides a top-down view of three sets of field lines with selected R_{SOL} of 1.57 m, 1.55 m and 1.51 m, which lie between the antenna radius of 1.575 m and the last closed flux surface (LCFS) radius of 1.477 m. Each set contains twenty field lines that cover the 90° toroidal span of the antenna. The points at which the field lines strike the lower divertor are denoted by squares. Although the antenna spans 90°, the lines converge radially as they wind around the center column, and lines starting closer to the LCFS strike the divertor farther in radially and wrap around the center column more toroidally, generating a spiral pattern similar to the visible-camera image in Fig. 1.

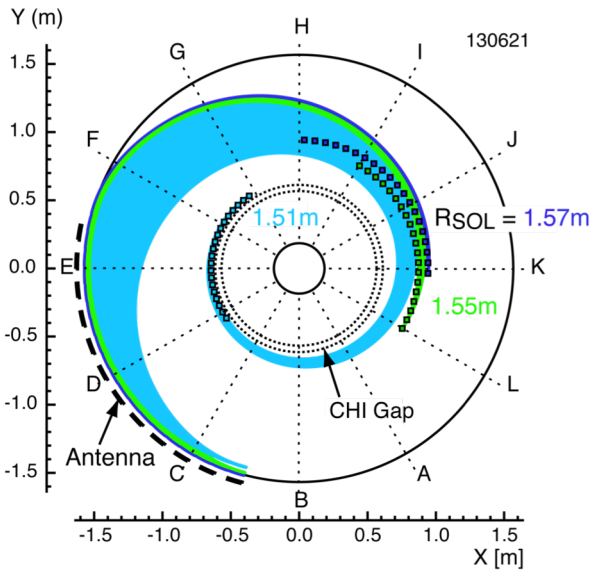

Figure 3. Field lines mapped between the midplane in front of the antenna and the lower divertor. The points at which each field line strikes the divertor are denoted by squares. The different colors denote lines that start at different radii at the midplane. Field lines starting more inboard of the antenna spiral around more and reach in further radially.

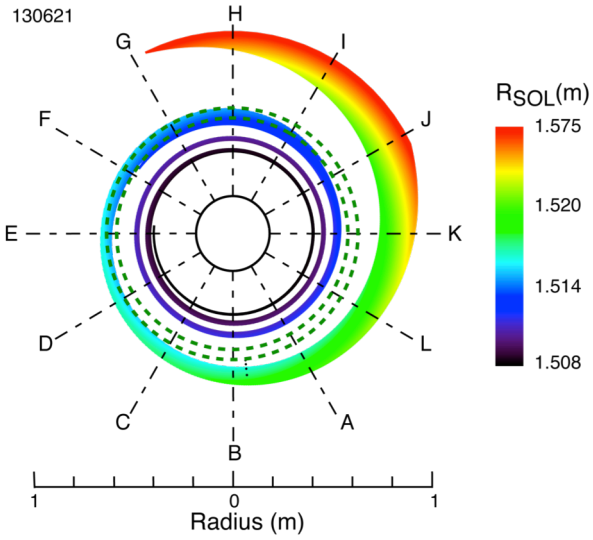

Figure 4. A large set of strike points defines a large spiral on the divertor floor. Field lines are tracked from the midplane in front of the antenna; the color-coding denotes the midplane radii of each line. The resulting spiral matches those seen in camera images (Fig. 1). The CHI gap is denoted by the dashed green circles.

The field-line mapping is compared with diagnostic measurements in the divertor region, so it is often sufficient to know only the strike points of the field lines rather than the entire trajectories. Figure 4 plots these strike points on the lower divertor floor for a much-denser set of field lines that includes many different R_{SOL}; the color-coding denotes the midplane radius of the field line from which each strike point originated. The set of strike points forms a spiral

as is observed experimentally. It is important to not confuse this spiral, formed by a collection of field-line strike points, with the spiraling SOL field-line trajectories shown in Fig. 3. The strike-point positions allow quantitative comparisons of RF-induced effects with the field-line mapping.

2.2. Comparison of field-line mapping to diagnostic measurements

Previous comparisons of the field-line mapping to diagnostic measurements showed that the HHFW power flow through the SOL is largely field-aligned [12]. The RF-spiral moves across the divertor when the magnetic pitch of NSTX is changed as is observed in visible-camera images and in diagnostic signals such as for Langmuir probes and current-sensing tiles. The strike points generated by field-line mapping exhibit this motion and, in fact, reveal that the spiral movement is actually a rotation of the spiral due to the altered magnetic pitch. Also, the calculated strike points lie over the Langmuir probes and current-sensing tiles on shots for which these diagnostics show a strong response to the RF pulse. Thus, these experimental observations support the conclusion that the HHFW power flow through the SOL from the antenna to the divertor region is along the magnetic field.

IR camera measurements of RF power deposition on the upper and lower divertor regions also agree with the field-line-mapping spiral patterns [15]. The IR cameras are located at Bay I for the lower divertor region and at Bay G for the upper divertor region [16]. This paper focuses on the lower divertor results. Figure 5 shows heat-deposition profiles along an approximately radial sight line at Bay I for two shots under identical conditions: shot 130621 with 1.8 MW of HHFW power with -90° phasing between antenna current elements (k_ϕ = -8 m^{-1}), and reference shot 130617 with no HHFW power. Subtracting the two heat profiles gives the RF-induced component of the heat-deposition profile, del Q. The relatively large negative dip in del Q near R_{div} ~ 0.4 m in Fig. 5(a) is most likely due to a shift in plasma exhaust in the vicinity of the vessel outer strike radius due to RF core heating; this shift makes the subtraction inaccurate in the vicinity of the vessel outer strike radius. The subtraction is valid elsewhere and three RF-induced heat peaks are clearly resolved. There is significant heat deposition at large radii, 0.85 m – 1.1 m, well outboard of the outer vessel strike radius. This location is in good agreement with location of the outer band of the strike points shown in Figs. 5(b) and 5(c) for the equilibrium fits EFIT02 [17] and LRDFIT04 [18], respectively. The second pass of the spiral is just inboard of the CHI gap at 0.53 m – 0.6 m, and the corresponding heat deposition is much weaker. An additional heat peak with larger amplitude is clearly resolved at an inner radius of 0.45 m, corresponding to a third crossing of the spiral at Bay I. The SPIRAL results also indicate additional heat peaks close to the outer vessel strike radius that are not resolved in

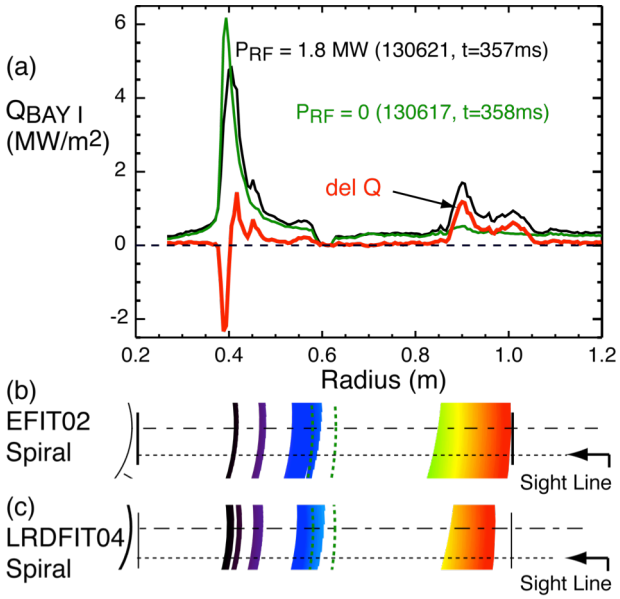

Figure 5. The field-line strike points agree well with the radial locations of peak RF power deposition measured with IR cameras. (a) An IR radial heat-flux profile at Bay I both with RF (black) and without RF (green). The subtraction of the two gives, del Q, the RF-power depositon (red). Computed strike points at Bay I with (b) EFIT02 and (c) LRDFIT04, are in reasonable agreement with heat-peak radii.

Fig. 5(a). The amplitude of the resolved heat peaks will be related to the midplane power-deposition profile in Sec. 3.

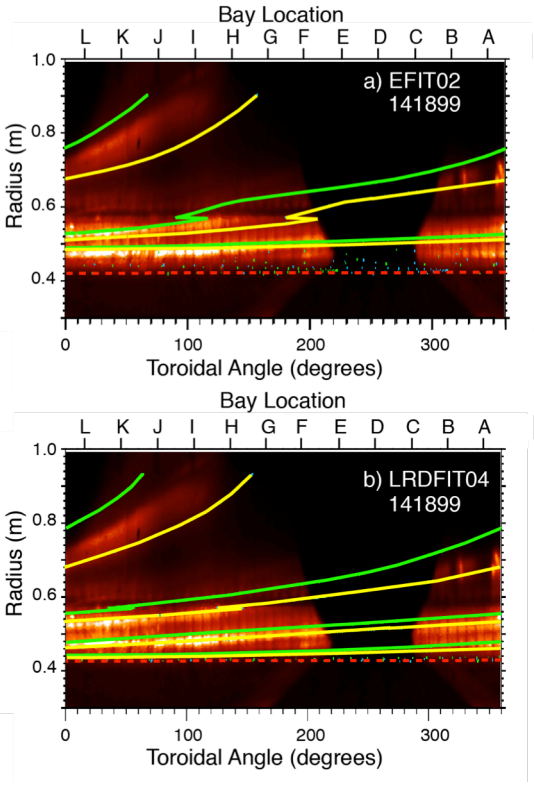

Figure 6. Different equilibrium fits give different field-line mappings. Here, a divertor-camera image of Li I emission is overlayed with field-line strike points from (a) EFIT02 and (b) LRDFIT04. Green points denote field lines from the right side of the antenna, and yellow points from the left hand side, so the RF power deposition occurs between the yellow and green points. The EFIT02 strike points match the RF streak well at outer radii but not close to the LCFS. LRDFIT04 generally matches the streak but not as well at larger radii.

The accuracy of the field-line mapping is limited by the accuracy of the equilibrium fits used. In Fig. 5, the LRDFIT04 spiral segments are shifted slightly to smaller R relative to the EFIT02 segments. Another example is given in Fig. 6 where overlays of strike points are compared with lower-divertor visible (Li I) emission images from shot 141899 [15] that have been inverted and plotted as major radius versus toroidal angle [19]. The upper figure contains strike points calculated using EFIT02 while the bottom figure uses LRDFIT04. The EFIT02 strike points fit the RF spiral better at outer radii and just inside the CHI gap but eventually deviate at inner radii. LRDFIT04 does not fit as well at outer radii but fits better as the outer vessel strike radius is approached. The strike points at inner radii come from field lines close to the LCFS that make many loops around the X-point, so any errors from the fits are sampled repeatedly for such field lines. Thus, the field-line mapping can be expected to be least accurate in the vicinity of the outer vessel strike radius. These differences are relatively small and do not alter the conclusion that the field-line strike points match the IR deposition measurements well. However, they demonstrate that the codes are sensitive to relatively small uncertainties in the equilibrium reconstructions; this could be important in general, for example in specifying exactly the location of the outer vessel strike radius.

3. Power-deposition profile at the midplane

Given the field-line mapping linking the SOL midplane to the divertor floor and that the HHFW power flow to the divertor region is primarily along field-lines, we can map the lower-divertor heat flux back to the midplane. This gives a radial profile of the HHFW power coupled to different field lines in the SOL and shows that the power coupled is relatively high both near the antenna and also the LCFS but drops in between. This profile indicates a radial standing fast-wave pattern across the SOL. We repeat the calculations for ELMy H-mode plasma shots and reach the same conclusion but with more resolution near the LCFS.

3.1. Calculating the Midplane Power Deposition

To compute the power flux coupled at the midplane, Q_{SOL}, from the divertor heat flux, Q_{div}, we need both the magnetic field-line mapping and the flux expansion factor. The latter is needed because the SOL flux surfaces are more spread out at the divertor than at the midplane due to the weakening of the poloidal field. Consider a differential surface element on the divertor

floor of width dR_{div} at a given divertor radius R_{div} and angular span $d\varphi$. Its image at the midplane under the field-line mapping results in another element of span $d\varphi$ but at a given SOL radius R_{sol} with width dR_{sol}. All the power flows within the flux tube connecting these two surface elements, so that for $dR << R$

$$Q_{SOL}R_{SOL}d\varphi dR_{SOL} = Q_{div}R_{div}d\varphi dR_{div}. \quad (1)$$

It is clear that

$$Q_{SOL} = Q_{div}\frac{R_{div}}{R_{SOL}}\frac{dR_{div}}{dR_{SOL}}, \quad (2)$$

where in Eq. (2) R_{div} is a function of R_{SOL} under the field-line mapping. Figure 7 plots ($R_{sol} - R_{lcfs}$) as a function of R_{div} as well as the flux expansion factor (dR_{div}/dR_{sol}) and the ratio R_{div}/R_{sol}. These allow the ratio Q_{sol}/Q_{div} of Eq. (2) to be computed and plotted in Fig. 7, which can then be used to calculate Q_{sol} for a given RF power deposition in the divertor region, Q_{div}. The translation factor Q_{sol}/Q_{div} is relatively large near the outer vessel strike radius (LCFS) and falls off with increasing radius. The jagged portions in Fig. 7 are due to the CHI gap.

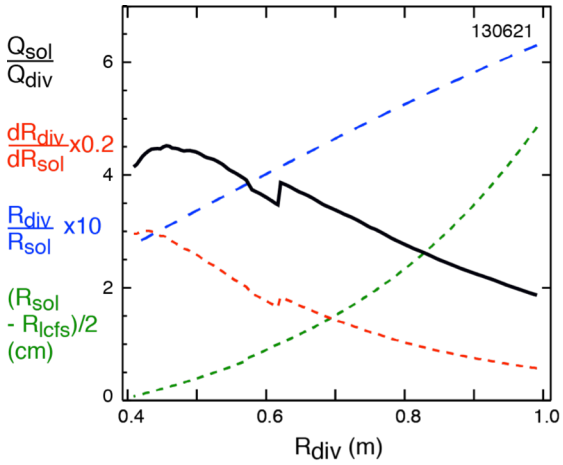

Figure 7. Solid black: the Q_{sol}/Q_{div} factor used to convert power deposited at the divertor region to power coupled along field lines at the midplane. Dotted red: flux expansion. Dashed blue: ratio of radius at divertor to radius at midplane. Dotted green: magnetic line mapping from divertor to midplane.

The IR camera used here only obtains data from Bay I (Fig. 5) and thus samples only a portion of the HHFW power flow, namely that along field lines whose strike points land at Bay I. Thus, regions of low heat flux shown in Fig. 5 do not correspond to midplane radii with low RF-power coupled; rather, the RF power flowing along such field lines lands off of Bay I in the lower divertor region. For this reason, only the local maxima of heat flux, whose field lines definitely land at Bay I, are mapped back to the midplane. While this limits the information obtained at the midplane, an indication of the power-coupling profile is still indicated, as shown in Fig. 8. The interesting conclusion is that the coupled power is relatively large both close to the antenna and also again near the LCFS for the ELM-free conditions of Fig. 5. This is reminiscent of a standing radial mode pattern and will be discussed further in the conclusions. Multiple IR cameras or a single wide-angle lens camera would allow a more complete recovery of the radial power-coupling profile in the SOL.

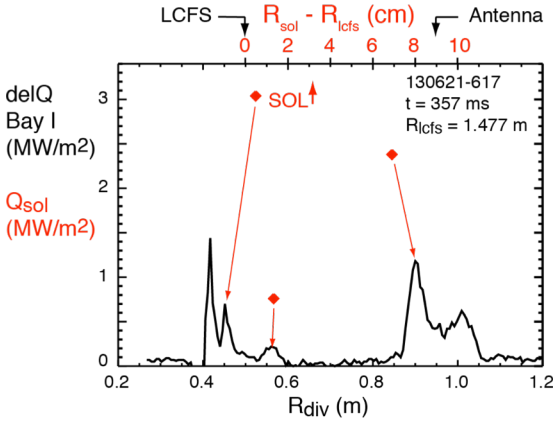

Figure 8. Using the conversion factor shown in Fig. 7, the IR measurement of RF heat deposition (black curve) can be converted to power coupled at the midplane (red points). This indicates that the coupled power peaks both close the antenna and also near the LCFS.

3.2. Midplane Power Deposition for an ELMy discharge

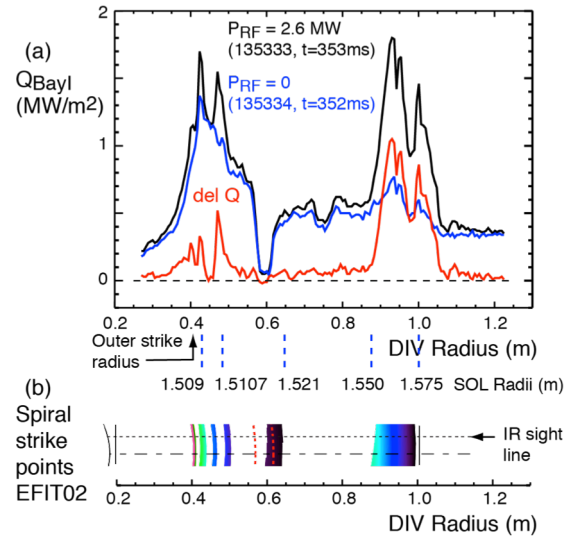

Figure 9. A comparison of the RF heat position for an ELMy H-mode plasma against field-line strike points. The multiple IR peaks close to the LCFS are consistent with the multiple passes of the computed strike-point spiral and have the same general location. The conditions are for shot 135333 are ϕ_{ANT} = -90°, P_{NB} = 2 MW, I_P = 0.8 MA, B_t = 0.45 T.

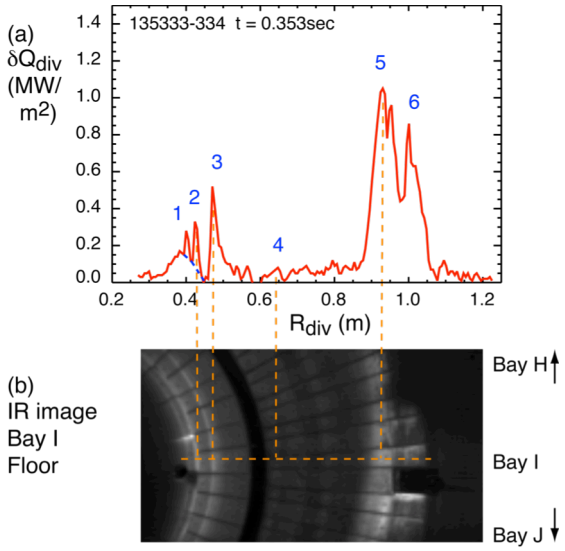

Figure 10. RF power deposition δQ_{div} for the ELMy H-mode plasma of Fig. 9 as viewed with (a) the IR camera data along the sight line at Bay I, and in (b) the IR camera image for shot 135333 for which the RF-induced streaks are clearly visible. Also shown in (b) is the sight line for the near radial profile in (a).

A clearer view of the hot spiral peaks near the outer vessel strike radius is obtained for an ELMy plasma as is shown in Fig. 9. The ELMs tend to raise the edge density and thus increase the edge losses [7]. The enhanced edge losses reduce the RF core heating so that the exhaust from the plasma around the outer vessel strike radius is less affected by the RF power reaching the core plasma inside the LCFS; however, the direct-RF power deposition in the SOL should be enhanced. The heat-flux peaks in the lower divertor are clearly resolved even near the outer vessel strike radius in Fig. 9. In fact, the RF-induced spiral streaks are clearly seen in the IR camera image shown in Fig. 10. These heat-flux peaks are mapped back to the midplane using Eq. (2) to give the Q_{sol} values in Fig. 11 versus the SOL radius, $\delta R_{sol} = R_{sol} - R_{LCFS}$. Here, it is resolved that the coupled power peaks a few millimeters outboard of the LCFS and a few centimeters inboard of the antenna but drops in between.

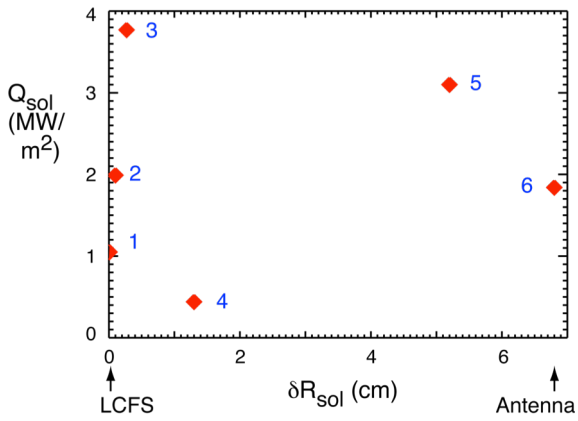

Figure 11. Calculated values of the power coupled at the SOL midplane, Q_{sol}, are shown for the peaks of the measured IR profile labelled 1 – 6 in Fig. 10. This data indicates that the power coupled in the SOL midplane peaks inboard of the antenna and again outboard of the LCFS. (R_{lcfs} = 1.508 m)

4. Conclusions

Given that the HHFW power coupled to the SOL flows from the NSTX antenna region to the divertor along field lines, the IR camera data has been mapped back to the midplane to obtain an estimate of the radial power coupling profile. In both cases analysed, the power couples strongly to field lines close to the antenna and to the LCFS but drops in between. This is

similar to a radial standing-wave pattern in a cavity and is indicative of fast-wave properties in the SOL. Another possible mechanism of direct SOL heating in the vicinity of the LCFS is PDI [6], but SPIRAL computations for the energetic ions produced show them to be mirror trapped away from the divertor regions, and the PDI losses do not appear to scale appropriately with the wavevector, k, to account for all losses [7]. While these losses to the divertor region have been studied on NSTX, a spherical torus with relatively high magnetic pitch, field-aligned RF-effects in the SOL have been observed under conventional tokamak conditions on Alcator C-Mod [20] and indicate these effects are common to fast-wave systems. Direct measurements of RF fields will be needed on NSTX-U to confirm experimentally that fast waves are propagating in the SOL. However, the SOL RF power flow results from NSTX provide a clear test for verifying advanced RF codes that treat the SOL region and that in turn can be used to theoretically understand the process(es) underlying the SOL power flow. Such a verification will also validate the use of advanced RF codes to predict and possibly minimize SOL power losses to the divertor region on ITER.

* This work is supported by USDOE Contract No. DE-AC02-09CH11466.

References

[1] Swain, D. W. and Goulding, R. H., *Fusion Eng. Des*. **82** (2007) 603.

[2] P. Jacquet *et al*., *Nucl. Fusion* **51** (2011) 103018.

[3] D.A. D'Ippolito *et al*., *Nucl. Fusion* **38** (1988) 1543.

[4] J.R. Wilson *et al*., *AIP Conf. Proc*. **787** (2005) 66.

[5] T.M. Biewer *et al*., *Phys. Plasmas* **12** (2005) 056108.

[6] C.C. Petty *et al*., *Nucl. Fusion* **39** (1999) 1421.

[7] J.C. Hosea *et al*., *Phys. Plasmas* **15** (2008) 056104.

[8] C.K. Phillips *et al., Nucl. Fusion* **49** (2009) 075015.

[9] J.C. Hosea *et al*., *AIP Conf. Proceedings* **1187** (2009) 105.

[10] G. Taylor *et al*., *Phys. Plasmas* **17** (2010) 056114.

[11] R. Raman *et al*., *Nucl. Fusion* **41** (2001) 1081.

[12] R.J. Perkins *et al*., *Phys. Rev. Lett*. 109 (2012) 045001.

[13] G.J. Kramer *et al.,* submitted to *Plasma Phys. Contr. F*. (2012)

[14] D.L. Green *et al., Phys. Rev. Lett*. **107** (2011) 145001.

[15] R.J. Perkins *et al., 39th EPS Conference on Plasma Physics* **36F** (2012) P-1.011.

[16] D. Mastrovito *et al*., *Rev. Sci. Instrum*. **74** (2003) 5090.

[17] S. Sabbagh *et al., Nucl. Fusion* **41** (2001) 1601.

[18] J. Menard, private communication.

[19] F. Scotti *et al., Rev. Sci. Instrum*. **83** (2012) 10E532.

[20] S. Wukitch *et al., AIP Conf. Proc*. **933** (2007) 75.